AGU PUBLICATIONS

Global Biogeochemical Cycles

RESEARCH ARTICLE
10.1002/2015GB005313

Key Points:
- The IPCC inventory substantially underestimates the indirect emissions within the Corn Belt
- Indirect emissions were much greater in year 2011 than 2010 due to increased precipitation
- Indirect emissions reached a maximum in June while direct emissions reached a maximum in July

Supporting Information:
- Supporting Information S1

Correspondence to:
Z. Chen,
chen3274@umn.edu

Citation:
Chen, Z., et al. (2016), Partitioning N_2O emissions within the U.S. Corn Belt using an inverse modeling approach, *Global Biogeochem. Cycles*, *30*, 1192–1205, doi:10.1002/2015GB005313.

Received 23 OCT 2015
Accepted 29 JUL 2016
Accepted article online 8 AUG 2016
Published online 24 AUG 2016

Partitioning N_2O emissions within the U.S. Corn Belt using an inverse modeling approach

Zichong Chen[1], Timothy J. Griffis[1], Dylan B. Millet[1], Jeffrey D. Wood[1], Xuhui Lee[2], John M. Baker[1,3], Ke Xiao[1], Peter A. Turner[1], Ming Chen[1], John Zobitz[4], and Kelley C. Wells[1]

[1]Department of Soil, Water, and Climate, University of Minnesota, Twin Cities, Saint Paul, Minnesota, USA, [2]School of Forestry and Environmental Studies, Yale University, New Haven, Connecticut, USA, [3]United States Department of Agriculture, Agricultural Research Service, Saint Paul, Minnesota, USA, [4]Department of Mathematics, Augsburg College, Minneapolis, Minnesota, USA

Abstract Nitrous oxide (N_2O) emissions within the US Corn Belt have been previously estimated to be 200–900% larger than predictions from emission inventories, implying that one or more source categories in bottom-up approaches are underestimated. Here we interpret hourly N_2O concentrations measured during 2010 and 2011 at a tall tower using a time-inverted transport model and a scale factor Bayesian inverse method to simultaneously constrain direct and indirect agricultural emissions. The optimization revealed that both agricultural source categories were underestimated by the Intergovernmental Panel on Climate Change (IPCC) inventory approach. However, the magnitude of the discrepancies differed substantially, ranging from 42 to 58% and from 200 to 525% for direct and indirect components, respectively. Optimized agricultural N_2O budgets for the Corn Belt were 319 ± 184 (total), 188 ± 66 (direct), and 131 ± 118 Gg N yr^{-1} (indirect) in 2010, versus 471 ± 326, 198 ± 80, and 273 ± 246 Gg N yr^{-1} in 2011. We attribute the interannual differences to varying moisture conditions, with increased precipitation in 2011 amplifying emissions. We found that indirect emissions represented 41–58% of the total agricultural budget, a considerably larger portion than the 25–30% predicted in bottom-up inventories, further highlighting the need for improved constraints on this source category. These findings further support the hypothesis that indirect emissions are presently underestimated in bottom-up inventories. Based on our results, we suggest an indirect emission factor for runoff and leaching ranging from 0.014 to 0.035 for the Corn Belt, which represents an upward adjustment of 1.9–4.6 times relative to the IPCC and is in agreement with recent bottom-up field studies.

1. Introduction

As one of the most intensively managed agricultural areas in the world, the U.S. Corn Belt plays an important role in meeting global demands for corn, soybean, and biofuel production. To sustain this production, ~5.0 Tg of nitrogen (N) is applied as synthetic fertilizer to fields in the Corn Belt each year [*Millar et al.*, 2010; *Griffis et al.*, 2013]. Large inputs of synthetic N fertilizer and biological N fixation associated with legume cropping are directly related to increasing concentrations of atmospheric nitrous oxide (N_2O), a greenhouse gas with a 100 year average global warming potential 298 times larger than an equal mass of CO_2 [*Myhre et al.*, 2013].

Constraints on regional to continental scale N_2O budgets are needed to develop baseline emission estimates that can be used as a reference in order to inform and assess policy and mitigation strategies. Investigations using top-down or bottom-up methodologies have been used to estimate N_2O emissions [*Kort et al.*, 2008; *Miller et al.*, 2012; *Griffis et al.*, 2013]. Using a top-down constraint and short-term air flask observations, *Kort et al.* [2008] estimated that emissions over North America were up to threefold larger than from bottom-up inventories. With regional tall tower measurements and daily flask data, *Miller et al.* [2012] estimated that regional budgets were at least twofold larger than bottom-up inventories when performing geostatistical and Bayesian inverse analyses. Using 2 years of hourly tall tower observations, *Griffis et al.* [2013] applied atmospheric boundary layer approaches to estimate the N_2O budget within the U.S. Corn Belt. Their estimates agreed well with other top-down estimates based on inverse analyses [*Kort et al.*, 2008; *Miller et al.*, 2012], and were twofold to ninefold greater than bottom-up approaches. Based on a global analysis of N entering agricultural systems, *Crutzen et al.* [2008] and *Smith et al.* [2012] concluded that N_2O emissions would need to be twofold to 3.4-fold larger than current bottom-up inventories in order to match the observed changes in atmospheric N_2O concentration over the period 1860 to 2000. The large difference between top-down and bottom-up N_2O budgets at regional to continental scales implies that the emission inventories are not adequately accounting for N_2O sources. However, there is a good agreement between top-down and bottom-up methodologies at the global scale [*Del Grosso et al*., 2008; *Thompson et al*., 2014].

Agricultural N_2O emissions arise from direct emissions from fertilized soils and through two indirect pathways: (i) from the deposition of NH_3 and NO_x volatilized from synthetic fertilizer and manure; and (ii) from the leaching and runoff of fertilizer and manure N, mainly as nitrate (NO_3^-). Previous studies from various agricultural fields within Minnesota indicate that direct N_2O emission is about 1.3% of applied synthetic N and in excellent agreement with the Intergovernmental Panel on Climate Change (IPCC) direct emission factor [*Fassbinder et al*., 2013; *Griffis et al*., 2013]. A recent meta-analysis has shown that this emission factor is well constrained but increases nonlinearly as N addition exceeds crop demand [*Shcherbak et al*., 2014]. One of the largest sources of uncertainty in the bottom-up estimates is related to the indirect sources from agricultural ecosystems. For example, indirect emissions from leaching and runoff have an emission factor range of 0.0005 to 0.025 (a fiftyfold range) due to a lack of observations at the appropriate spatial and temporal scales [*Nevison*, 2000; *Outram and Hiscock*, 2012; *Turner et al*., 2015].

Agricultural drainage systems (i.e., tile lines and ditches, and surface waters), necessary to support crop production in the U.S. Corn Belt, have shown the potential for large episodic emissions. The indirect emissions from these streams remain poorly quantified at the appropriate spatial scales and are thought to contribute substantially to regional emissions [*Beaulieu et al*., 2011; *Outram and Hiscock*, 2012; *Turner et al*., 2015]. Approximately 2.3 million hectares of land have been drained for agriculture in Minnesota. These fine-scale drainage features represent a key hydrological conduit for the transport of N [*Alexander et al*., 2000]. *Turner et al*. [2015] analyzed N_2O emissions as a function of Strahler stream order in southern Minnesota and found that headwater streams (i.e., stream order of 1) were the strongest sources, emitting 60% of the riverine budget. Their scaling suggested that by accounting for emissions from zero-order streams that the regional N_2O budget would more than double. Further, these indirect emissions may become more important because drainage and stream flow have both increased within the region over the last 50 years [*Baker et al*., 2012].

In this paper we employed an inverse analysis to simultaneously constrain the direct and indirect N_2O sources within the U.S. Corn Belt. Tall tower measurements were used to provide high-resolution information with a large-scale footprint that is highly sensitive to emission from the US Corn Belt. A Bayesian inverse analysis was adopted to identify and constrain the N_2O budget, sources, and sensitivity to environmental drivers. Here we address the following questions: (1) Can Bayesian inverse modeling be used to objectively constrain the direct and indirect sources contributing to N_2O emissions in the US Corn Belt? (2) To what sources are observed tall tower N_2O concentrations most sensitive? (3) What are the seasonal patterns of the direct and indirect N_2O emissions? (4) How do the environmental factors (e.g., precipitation, air temperature, soil moisture, and surface runoff) influence N_2O emissions from direct versus indirect emissions?

2. Methods

2.1. Approach Overview

The inverse approach employed in this study is outlined in Figure 1. The Weather Research and Forecasting (WRF) model version 3.5 [*Zhao et al*., 2009; *Nehrkorn et al*., 2010; *Jeong et al*., 2012] provides the conditions of wind, atmospheric stability, and planetary boundary layer (PBL) height to drive the Stochastic Time-Inverted Lagrangian Transport (STILT) model [*Gerbig et al*., 2003; *Lin et al*., 2003, 2004], which was used to estimate the tall tower concentration source footprint. The source footprint was multiplied by a priori emission estimates derived from a variety of sources (see section 2.5 for details), which is added to the background concentrations, to obtain an initial guess of N_2O concentrations at the tall tower receptor. With these initial estimates and the tall tower concentration observations, a Bayesian inverse model was used to optimize the a priori emissions along with the relative contributions of direct and indirect sources.

2.2. Study Domain

Our study domain is focused on the US Corn Belt and includes the major corn/soybean production systems in Minnesota, Illinois, Indiana, Iowa, Missouri, Ohio, South Dakota, Nebraska, and Wisconsin. The N_2O concentration measurements were made at the University of Minnesota tall tower Trace Gas Observatory (KCMP tall tower,

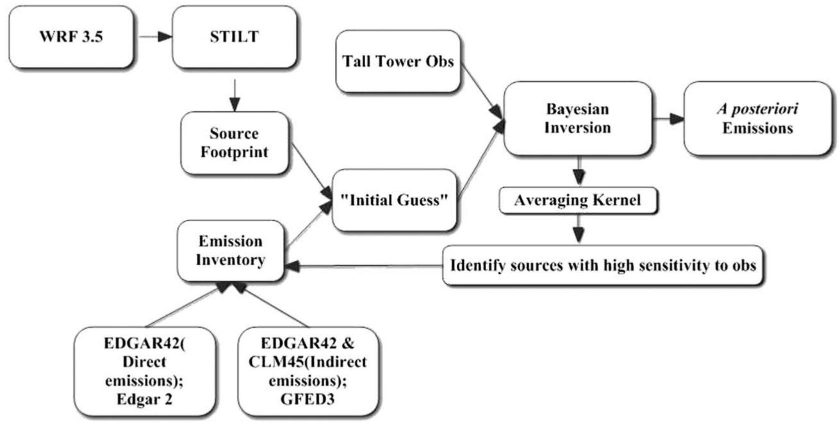

Figure 1. Overview of the inverse modeling approach used to estimate direct and indirect agricultural N_2O emissions.

44.689°N, 93.073°W; 244 m height) over a 2 year period (2010 and 2011). The KCMP tower is located approximately 25 km south of Minneapolis—St. Paul, MN. In the vicinity of the tower, agriculture represents approximately 46% of the land use and is representative of the larger U.S. Corn Belt region [*Zhang et al*., 2014].

2.3. Tall Tower N_2O Measurements

During 2010–2011, air samples were analyzed at the tall tower at heights of 32, 56, 100, and 185 m. Air was pulled continuously through each inlet to the base of the tower and then subsampled at 3 standard liters per minute using a custom designed manifold. N_2O mixing ratios were measured using a tunable diode laser (TGA100A, Campbell Scientific Inc., Logan, Utah, USA) that was housed in a temperature-controlled building. Hourly calibrations were performed using a zero and span gas. The span gas was traceable to the National Oceanic and Atmospheric Administration (NOAA)-Earth System Research Laboratory. The hourly TDL calibration precision, estimated using the Allan variance technique [*Werle et al*., 1993], was estimated to be 0.5 ppb [*Griffis et al*., 2013]. Following calibration, hourly average N_2O concentrations were computed. Previous work has employed N_2O measurements from the KCMP tower to estimate the total regional N_2O source [*Griffis et al*., 2013] and as part of a global analysis to assess our current ability to constrain N_2O sources worldwide [*Wells et al*., 2015]. Further details regarding the sampling system and calibration can be found in *Griffis et al*. [2010, 2013].

2.4. Source Footprint Simulations

The source footprint function delineates areas that influence the tall tower observations [*Kim et al*., 2013]. The STILT model computes the upstream influence on a measurement site by releasing a suite of particles from the receptor (tall tower air intake at 100 m) and following their trajectory backward in time. The time- and volume-integrated footprint function is quantified by tallying the total amount of time each particle spends in a volume element over a time step, normalized by the total amount of particles. Molar mass and density of air and the mixing height are accounted for in the function in order to scale all the particles to represent the entire vertical profile [*Lin et al*., 2003; *Gerbig et al*., 2003; *Lin and Gerbig*, 2005]. Multiplying the source footprint by the a priori emissions and summing over all locations provides an estimate of the tall tower mixing ratios.

We simulated wind fields using the WRF3.5 and interpolated them to the explicit location of each particle. The WRF3.5 was set up using three nests at 27 km, 9 km, and 3 km grid spacing. The outermost domain covers North America, and each domain was centered on the tall tower. The simulations used WRF Single-Moment three-class (WSM3) simple ice microphysics scheme [*Hong et al*., 2004], Kain-Fritsch convective scheme [*Kain*, 2004], and the Yonsei University (YSU) scheme coupled to the Noah land surface model for the planetary boundary layer (PBL) processes [*Hong et al*., 2006]. Initial and boundary conditions were provided by the National Center for Environmental Prediction Final Analysis (1° × 1°), with a 6 h interval.

In this study, we released 500 particles per hour from the KCMP tall tower at a height of 100 m for the years of 2010 and 2011 and transported them backward for 7 days to ensure that the trajectories adequately represented source contributions from within the U.S. Corn Belt. Furthermore, we used observations from the

NOAA Carbon Cycle and Greenhouse Gases program [*Dlugokencky et al*., 1994] near the outer edge of the source footprint to represent the background mixing ratios. These observations are from discrete air samples collected approximately weekly in flasks at 77 sites and are zonally and monthly averaged at 4° latitudinal resolution [*Wells et al*., 2015].

2.5. A Priori Emissions

We used EDGAR42 (Emission Database for Global Atmospheric Research, version 4.2, 2011, http://edgar.jrc.ec.europa.eu), to provide a priori annual N_2O emissions. Different sources in the inventory were tracked as separate tagged tracers in our simulation, with the sum of these equal to the total ambient N_2O mixing ratio. EDGAR42 represents the source emission at a spatial resolution of $0.1° \times 0.1°$. Here we reorganized the anthropogenic sources of N_2O into five categories and included two natural source categories to represent emissions including the following: (1) Direct emissions from agricultural soils (*dirA*), including synthetic N fertilizer, manure management, and crop residues; (2) indirect emissions from leaching/runoff in agriculture (*indA*), provided by CLM45-BGC (Community Land Model coupled to Biogeochemistry) [*Oleson et al*., 2013]; (3) solid waste and wastewater (*waste*); (4) industrial processes (noncombustion) (*industry*); (5) fuel combustion and fugitive emissions from fuel (*energy*); (6) natural emissions (*natsoil*) from nonagricultural soil provided by EDGAR2; and (6) biomass burning (*BB*) from Global Fire Emissions Database, version 3, 2011, (http://www.globalfiredata.org).

Initially, we used the indirect emissions from agriculture from the leaching/runoff category from EDGAR42. However, since dirA and indA from EDGAR42 are both calculated using the IPCC emission factor (EF) approach they were found to be highly correlated ($r^2 = 0.99$), and therefore, cannot be considered independent variables in our optimization. To address this concern we used indA obtained from the CLM45-BGC. In CLM45-BGC, the Century N model [*Parton et al*., 1996, 2001; *DelGrosso et al*., 2000] was used to simulate the soil NO_3^- pool.

Since the CLM45-BGC model does not provide indA directly, we estimated it by multiplying the soil NO_3 pool losses to leaching and runoff by the IPCC EF_5 default value of 0.0075 [*de Klein et al*., 2006]. The CLM45-BGC model was run for 2010 with and without crops. The crop-on model simulated N leaching and runoff from both agricultural and natural soils, while the crop-off model only simulated N leaching and runoff from natural soils. By taking the difference of these two simulations, we estimated the N leaching and runoff attributed to agricultural soils. Next, we applied the EF_5 to obtain the indirect emissions from agriculture. Here we assume that N leaching and runoff from the CLM45-BGC is correct.

An important point is that indirect N_2O from volatilization and redeposition is not explicitly represented in our a priori emissions. The IPCC methodology [*De Klein et al*., 2006] does, however, account for agricultural N_2O emissions arising from the volatilization and redeposition of reactive N. In our methodology all indirect emissions are allocated to one source category, indA. We attribute our indirect emission estimates to the leaching and runoff source category, because we have observed high fluxes from surface water systems within the region [*Turner et al*., 2015]. However, it is possible that these aquatic emissions arise from amplification of the N cycle owing to both leaching/runoff and deposition. Therefore, our emission factor may be overestimated and should be taken as a conservative upper bound.

2.6. Bayesian Inversion Methods

We defined the mixing ratio observed at the tall tower, *Y*, and subtracted the background value as defined in section 2.4. Next, a scale factor Bayesian inverse method was applied for each month (April to October, in 2010 and 2011, respectively). As described in *Gerbig et al*. [2003], *Zhao et al*. [2009], and *Jeong et al*. [2012], *y* can be modeled as

$$\mathbf{y} = \mathbf{K\Gamma} + \boldsymbol{\varepsilon} \tag{1}$$

where *y* is the observed minus background mixing ratios; Γ is the scaling factors for different source types; *K* is the Jacobian matrix, representing the sensitivity of the observation variables to the specific source types; and ε is the system error, which consists of instrumental and model errors. In our case, the columns of *K* correspond to the mixing ratios for each of the source types being optimized, and Γ consists of the a posteriori scale factors for the seven source types.

Applying Bayes' theorem, along with a normal distribution assumption, the maximum a posteriori (MAP) solution of Γ *is* to minimize the cost function $J(\Gamma)$:

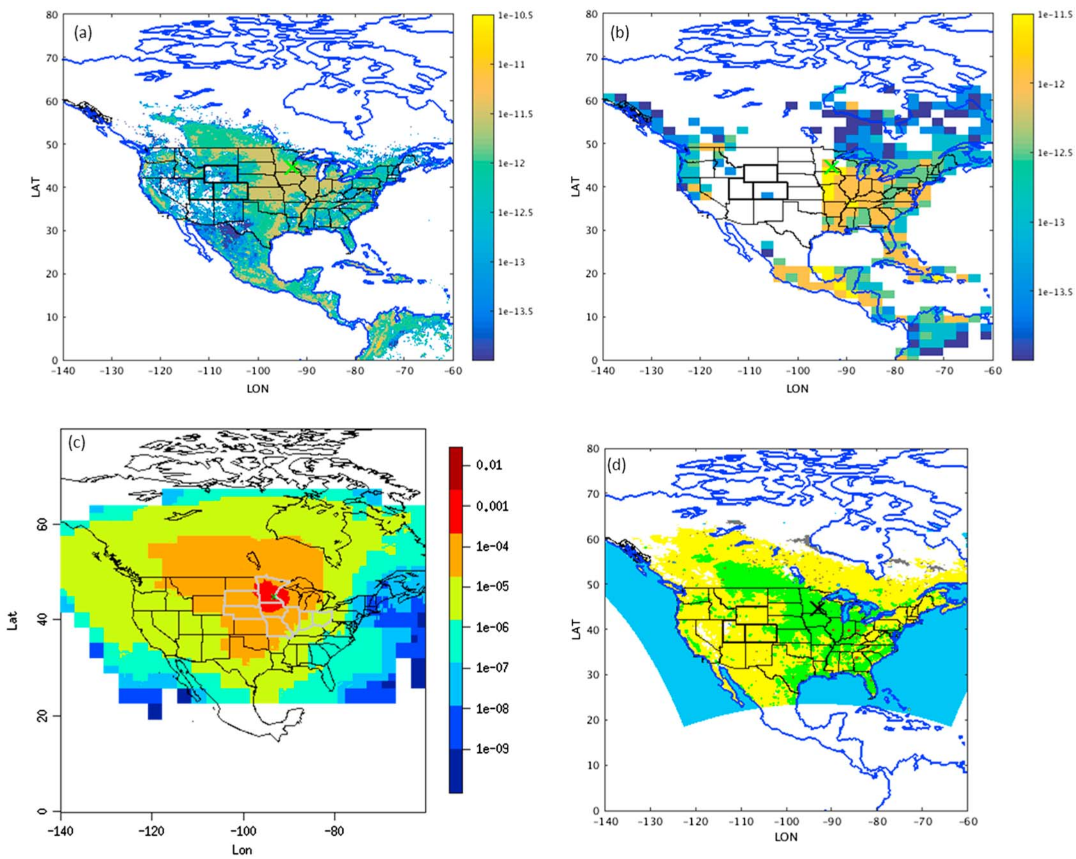

Figure 2. (a) The a priori annual average direct N_2O emissions from agriculture (unit is $\log_{10}(\mathrm{kg\,m^{-2}\,s^{-1}})$); (b) a priori annual average indirect N_2O emissions from agriculture (the coastlines are denoted by blue lines, and the US States are denoted by black lines); (c) annual average source footprint of the tall tower (units are $\log_{10}(\mathrm{ppm\,\mu mol^{-1}\,m^2\,s})$); the U.S. Corn Belt is denoted by gray lines; (d) land use distribution from U.S. Geological Survey (red, green, yellow, gray, and light blue colors denote the urban, agricultural soils, natural soils, wetlands, and water bodies, respectively).

$$\mathbf{2J}(\mathbf{\Gamma}) = (\mathbf{y} - \mathbf{K\Gamma})^{\mathbf{T}}\mathbf{S}_{\varepsilon}^{-\mathbf{1}}(\mathbf{y} - \mathbf{K\Gamma}) + (\mathbf{\Gamma} - \mathbf{\Gamma_a})^{\mathbf{T}}\mathbf{S_a}^{-\mathbf{1}}(\mathbf{\Gamma} - \mathbf{\Gamma_a}) \tag{2}$$

where S_ε and S_a are the observational and a priori error covariance matrices and each element of $\Gamma_a = 1$. The solution to $\nabla\Gamma J(\Gamma) = 0$ is then given by

$$\mathbf{\Gamma_{post}} = \left(\mathbf{K^T S_\varepsilon^{-1} K} + \mathbf{S_a}^{-\mathbf{1}}\right)^{-\mathbf{1}}\left(\mathbf{K^T S_\varepsilon^{-1} y} + \mathbf{S_a}^{-\mathbf{1}}\mathbf{\Gamma_a}\right) \tag{3}$$

Observational errors consist of measurement and modeling errors. The measurement error ascribed to the TDL was based on the estimate of calibration precision, which was 0.5 ppb.

The measurement uncertainty from observations of background mixing ratios is 0.4 ppb, based on recommendations from the data providers [*Wells et al.*, 2015]. Therefore, we assign an uncertainty of 0.4 ppb for background mixing ratios.

Since STILT releases a finite number of particles (500 particles in the simulations presented here), we follow previous work [*Gerbig et al.*, 2003; *Miller et al.*, 2008] and assign an uncertainty of 13% for the simulated back trajectories. The uncertainty associated with the simulation of PBL height (i.e., the effect of PBL height on concentrations) was estimated from the monthly mean values of $|H_{obs} - H_{model}|/H_{obs}$. H_{obs} is the mixing height inferred from radiosonde observations [*Matross et al.*, 2006; *Miller et al.*, 2008; *Kretschmer et al.*, 2012; *Kim et al.*, 2013]. H_{model} is the mixing height from the WRF-STILT simulations, using Yonsei University [*Hong et al.*, 2006] and Mellor-Yamada-Janjic [*Janjic*, 2002] PBL schemes, respectively. The relative uncertainty estimated here is 21%. The modeling error ranges from 4 to 8 ppb and is much larger than the measurement error.

The uncertainties assigned to the a priori emissions shown in Figures 2a and 2b were obtained from the literature [*De Klein et al.*, 2006; *Shcherbak et al.*, 2014]. A recent meta-analysis found a nonlinear response in the EF for direct emissions from agricultural soils, however, they reported good agreement with the IPCC default value when N rates were within the range of typical values for the Corn Belt albeit with reduced uncertainty, which is ~66% when the N application rate is ~150 kg ha^{-1} [*Shcherbak et al.*, 2014]. The uncertainty in the indirect emissions was set at 401% by propagating assumed uncertainties of 327% in the default EF_5 and 233% for the amount of N in leaching/runoff [*de Klein et al.*, 2006]. Based on the IPCC recommendations, the uncertainties of industry, waste, energy, natsoil, and BB to the a priori emissions were 30%, 30%, 30%, 38%, and 30% in the default EFs, respectively [*Gómez et al.*, 2006]. Therefore, initial relative error estimates of 66%, 401%, 30%, 30%, 30%, 38%, and 30% were applied for dirA, indA, industry, waste, energy, natsoil, and BB, respectively, to construct the a priori error covariance (see supporting information for more details related to the Bayesian inversion).

We conducted two tests to evaluate the sensitivity of the Bayesian inversion to the a priori flux distribution and spatial aggregation errors. First, we examined the differences when using a relatively high spatial resolution (a priori inventory with a 0.1°×0.1° resolution) versus a lower spatial resolution (a priori inventory with a degridded 0.5°×0.5° resolution) flux inventory. Second, we perturbed the original spatial distribution of the a priori flux inventory with a random variable that varies in space, having a normal distribution with a mean of unity, and a standard deviation of 30%. Both tests indicated that the sensitivity of the inversion results to spatial resolution and source distribution were not statistically significant at the 5% significance level.

We acknowledge that our modeling framework has limitations associated with the assumptions of spatial distribution and source aggregation. We are depending on measurements from one point in space and, therefore, cannot solve independently for emissions from every model grid cell and time and individual source sector. This is a limitation of all similar atmospheric inversion studies and has been acknowledged previously [*Mikaloff Fletcher et al.*, 2004; *Carouge et al.*, 2010; *Bousquet et al.*, 2011].

2.7. Sensitivity to True Values

In order to identify the source types that contribute to the tall tower concentrations, we calculated the averaging kernel (AK) to quantify the sensitivity of the retrieved emissions to their true value [*Rodgers*, 2000; *Kim et al.*, 2013].

The Bayesian inverse framework constrains the source categories and provides optimized emissions using a cost function analysis. The AK represents the sensitivity of the MAP solution, $\hat{x}$, to the true state, x (i.e., the true emissions from a specific source type):

$$\mathbf{A} = \mathbf{1} - \hat{\mathbf{S}}\mathbf{S_a}^{-1} = \frac{\partial \hat{\mathbf{x}}}{\partial \mathbf{x}} \tag{4}$$

where A is the averaging kernel and $\hat{S}$ and S_a are the a posteriori and a priori error covariance matrices, respectively. The AK is used to gain insights regarding (1) how sensitive are the tall tower measurements to some specific source types and (2) whether the source types will be resolved from one another. This type of sensitivity analysis allows identification of the source types contributing to the tall tower N_2O concentrations [*Heald et al.*, 2004; *Kim et al.*, 2013].

2.8. N_2O Emission Budgets

Following the optimization, we obtained the total N_2O budget (B_j) for each source type j according to

$$\mathbf{B_j} = \sum_{\mathbf{i=1}}^{\mathbf{n}} \left(\mathbf{f_j} \times \mathbf{S} \times \mathbf{t}\right) \tag{5}$$

where n is the number of grid cells within the U.S. Corn Belt. For each grid cell, f_j is the a posteriori N_2O emissions (kg N m^{-2} s^{-1}) for source type j, where the a posteriori emissions are the a priori emissions multiplied by the corresponding scaling factor (Γ), S is grid cell area (m^2), and t is time (s).

ArcGIS (v.10.1, Environmental Systems Research Institute, Redlands, California, USA) was used to identify grid cells within the Corn Belt and to compute the areas of each grid cell intersected by the Corn Belt. The intersection function was applied for the nine States (South Dakota, Nebraska, Kansas, Missouri, Minnesota, Iowa, Illinois, Ohio, and Indiana) to obtain all the grid cell areas over the Corn Belt.

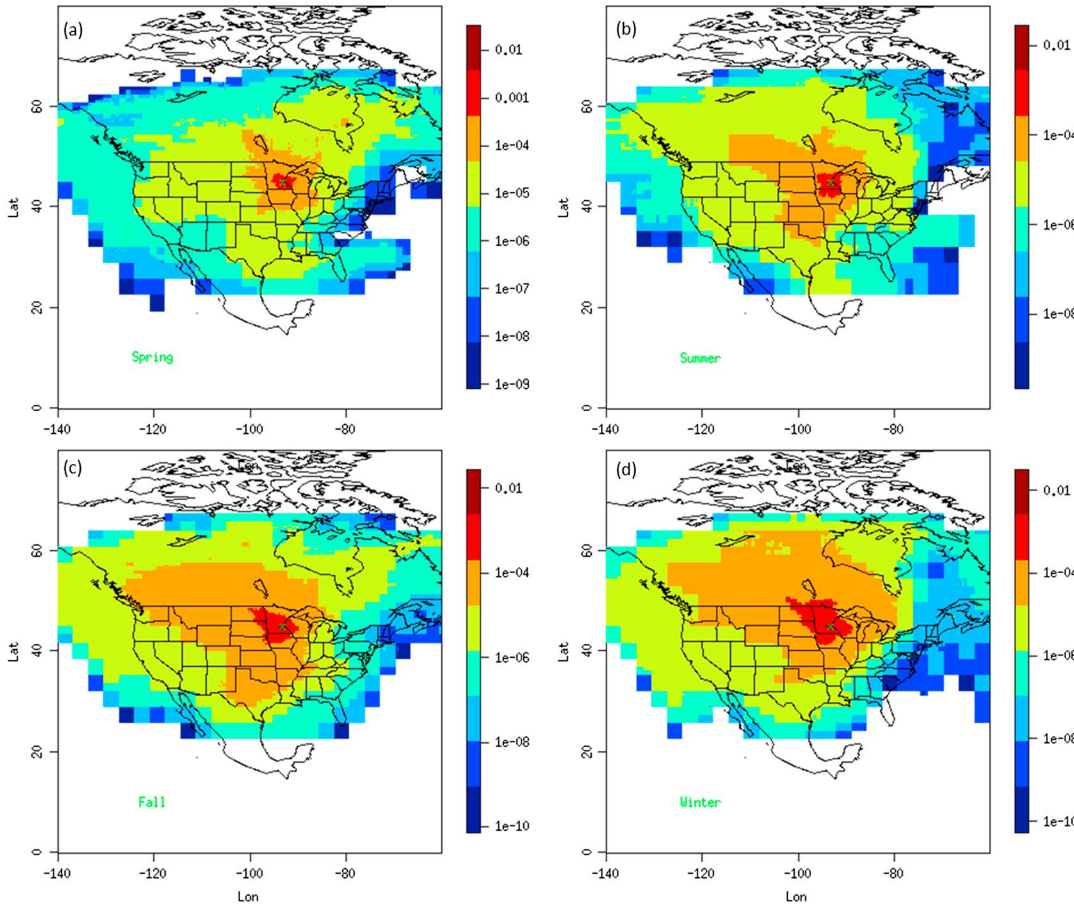

Figure 3. Average seasonal source footprints for measurements at the KCMP tall tower (indicated by crosses), 2010 (units: $\log_{10}$(ppm μmol^{-1} m^2 s)). (a) Spring: March, April, and May; (b) summer: June, July, and August; (c) fall: September, October, and November; (d) winter: December, January, and February.

3. Results and Discussion

3.1. Source Footprint of the Tall Tower

The tall tower concentration source footprints (Figures 2c and 3) indicate that the measurements were influenced by sources from within the U.S. Corn Belt. Figure 3 shows the season-averaged footprint function at the KCMP tall tower for 2010 as derived from the WRF-STILT model. The source footprint at the tall tower reached north to Canada and extended south to the Gulf of Mexico. *Kim et al*. [2013] and *Hu et al*. [2015] also concluded that the KCMP tall tower measurements (at the 185 m level) were representative of surface influence at the continental scale.

Areas where the footprint strength was greater than 1*e*−4 ppm μmol^{-1} m^2 s^{-1}, representing the dominant surface influence to the tall tower observations, were defined as intense footprint zones. These intense footprint zones encompassed the Corn Belt and extended north to southern Canada. Further, these analyses show that natural sources outside of the Corn Belt can also have an important influence on the tall tower observations. Figure 2d shows the land use categories of our study domain [*Homer et al*., 2011]. Statistical analysis of the land use within the intense footprint zone indicates that agricultural soils, natural soils, urban areas, and water bodies accounted for 81.6%, 12.0%, 0.5%, and 1.4%, respectively. Based on source footprint analyses, the tall tower observations appeared to provide adequate representation of the emissions and transport of N_2O related to the U.S. Corn Belt.

3.2. A Priori and A Posteriori Emissions

In the first Bayesian inversion, seven source types were included in the optimization (as described in section 2.5). The AK obtained from this inversion (Table 1) revealed extremely weak sensitivities for the industry, energy,

Table 1. Averaging Kernel of the Source Types

Source Categories	dirA	indA	natsoil	Industry	Energy	Waste	BB
AK	0.81	0.90	0.93	0.002	0.002	0.005	0.002

waste, and biomass burning sources, indicating a very limited contribution from these source types to the tall tower observations. These source types, therefore, were not resolved by the tall tower observations. However, the sensitivity is strong for the direct and indirect agricultural sources and the natural sources. This is supported by the statistical analyses of the land use within the source footprint described above as well as previous investigations [*Miller et al*., 2012; *Saikawa et al*., 2013; *Griffis et al*., 2013]. The source categories to which measurements were insensitive were generally a result of extremely low emissions (e.g., biomass burning) or very limited area (e.g., industry). Agricultural soils and natural soils are key sources from within and outside of the intense footprint zones, respectively. Based on the low sensitivities as indicated by the AK and the land use analyses, the industry, energy, waste, and biomass burning source categories were eliminated from further consideration, and a second Bayesian inversion was performed where we included only the direct and indirect agricultural and natural soil source categories. The annual average a priori emissions for this second inversion were 0.12 (direct), 0.04 (indirect), and 0.04 (natural soils) nmol m^{-2} s^{-1}, respectively, which are represented spatially in Figures 2a and 2b. This second inversion yielded the final optimized a posteriori emission estimates.

To probe the degree that the a priori error construction influenced the optimized emissions, we performed a wide range of sensitivity studies by varying the a priori errors of 46–66% (direct) and 300–400% (indirect) in the in the Bayesian inversion (Table 2). The a posteriori errors were significantly reduced in both direct and indirect emissions in the cost function analysis, indicating a robust constraint of the Bayesian inverse approach. Our best estimate suggests that annual mean (± the a posteriori error) emissions in total, direct, and indirect agricultural sources were 0.30 ± 0.16, 0.18 ± 0.05, and 0.12 ± 0.11 nmol m^{-2} s^{-1} in 2010 and 0.44 ± 0.27, 0.19 ± 0.05, and 0.25 ± 0.22 nmol m^{-2} s^{-1} in 2011, respectively.

The relative uncertainty from natural soils reduced significantly from 38% to ~10%, suggesting a robust constraint. To investigate the impact of natural soils to agricultural sources, in the a priori emissions, a sensitivity test was performed by (i) increasing the natural soil source by 50% and (ii) decreasing the natural soil source by 50%. The results indicated that natural soils had little impact on both direct and indirect emissions from agriculture in the optimization. The optimized natural soils emissions were ~1.8 times larger than indicated from EDGAR2 within the Corn Belt and is consistent with the findings of *Wells et al*. [2015].

The a posteriori direct emissions were 1.5- to 1.6-fold larger than the IPCC bottom-up approach, suggesting an EF ranging from 1.5% to 1.6%, in close agreement with recent studies using a nonlinear response model [*Grace et al*., 2011; *Shcherbak et al*., 2014]. The a posteriori indirect emissions were 2.4- to 5.1-fold larger than from IPCC EF approach, providing further support [*Outram and Hiscock*, 2012; *Griffis et al*., 2013; *Turner et al*., 2015] that the indirect emissions are substantially underestimated by the IPCC bottom-up approach for this region.

3.3. Seasonal and Interannual Variations

As shown in Figure 4, there were clear seasonal and interannual variations in the a posteriori emissions. In both years, direct emissions began to increase after the snow melt, reached the peak in July, and then decreased

Table 2. A Posteriori Scale Factors and a Posteriori Errors for the Bayesian Inversion With Various Sensitivity Tests

A Priori Errors		Optimized Direct Emissions		Optimized Indirect Emissions	
Direct Emissions	Indirect Emissions	Scaling Factor	A Posteriori Error	Scaling Factor	A Posteriori Error
46%	300%	2.0	28%	4.7	90%
46%	350%	1.9	29%	5.0	102%
46%	400%	1.8	29%	5.3	100%
56%	300%	2.2	33%	4.3	91%
56%	350%	2.1	35%	4.7	102%
56%	400%	2.0	35%	5.0	101%
66%	300%	2.5	37%	4.0	94%
66%	350%	2.2	39%	4.3	100%
66%	400%	2.1	38%	4.6	95%

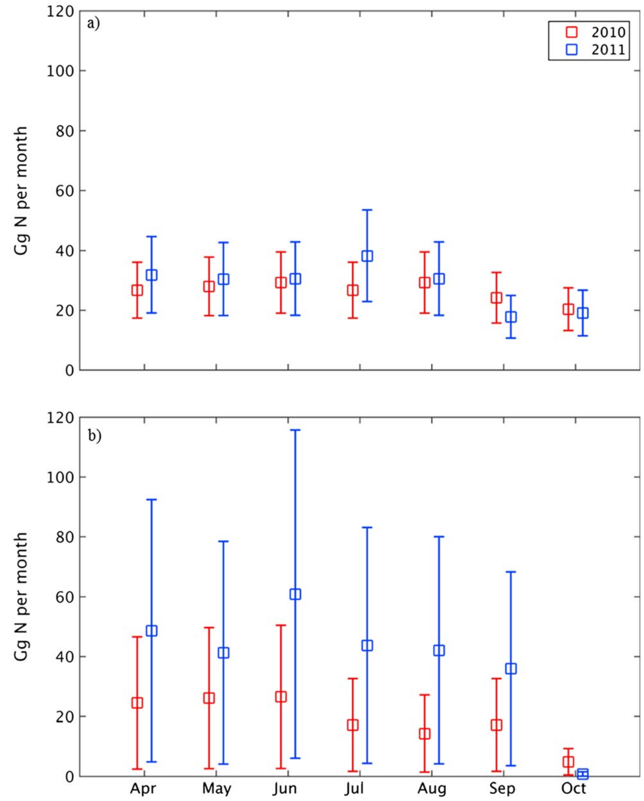

Figure 4. (a) Direct and (b) indirect N_2O emissions from agriculture within the U.S. Corn Belt for 2010 and 2011, respectively. Error bars represent the a posteriori uncertainties after optimization, for direct and indirect emissions.

through to the end of October. Interestingly, indirect emissions began to increase after the snow melt and reached their maximum in June. We attribute this to a combination of spring time fertilization throughout much of the Corn Belt and relatively high runoff and tile outflow. Summing over all seasons, our best estimates of the annual agricultural N_2O budgets for the Corn Belt were 319 ± 184 (total), 188 ± 66 (direct), and 131 ± 118 Gg N yr^{-1} (indirect) in 2010 versus 471 ± 326, 198 ± 80, and 273 ± 246 Gg N yr^{-1} in 2011. The direct and indirect budgets in 2011 increased by 5% and 108% over 2010, respectively. Hydrometeorological factors are explored to identify drivers that result in the large difference in N_2O emission partitioning.

Figure 5 shows a comparison of the N_2O budget and its partitioning between direct and indirect emissions obtained from a variety of independent methods. The Bayesian inverse approach estimates the N_2O budget in 2010 (316 ± 183 Gg N yr^{-1}), which is in reasonable agreement with tall tower atmospheric boundary layer approaches (420 ± 50 Gg N yr^{-1}) [*Griffis et al.*, 2013], as well as other top-down methodologies [*Kort et al.*, 2008; *Miller et al.*, 2012] but much larger than that derived from IPCC and other bottom-up approaches including EDGAR and Global Emission Initiative [*Bouwman et al.*, 1995]. The direct N_2O budget from the IPCC EF approach (120 Gg N yr^{-1}) is within the uncertainty range of our approach (188 ± 66 Gg N yr^{-1}). Therefore, for direct emissions, there is no significant difference between IPCC estimate and the Bayesian inversion. For indirect emissions, the IPCC estimate (52.3 Gg N yr^{-1}) is within the uncertainty range from our Bayesian inversion (131 ± 118 Gg N yr^{-1}). However, the optimization significantly reduces the uncertainties (Table 2) and places a better constraint on the indirect emissions. Furthermore, our findings also support the growing evidence [*Outram and Hiscock*, 2012; *Hinshaw and Dahlgren*, 2013; *Turner et al.*, 2015] that indirect emissions are higher than that estimated using the IPCC EF approach.

The direct emissions from the Bayesian inverse model suggest an EF ranging from 1.5% to 1.6%, 1.5 to 1.6 times larger than the default IPCC EFs. *Shcherbak et al.* [2014] showed that the N_2O emission factor increases nonlinearly as fertilizer N exceeds crop demand, and their nonlinear response model suggests a regional EF of 1.7%, assuming an average N application rate of 143 kg N ha^{-1} for the Corn Belt [*Griffis et al.*, 2013]. This is in

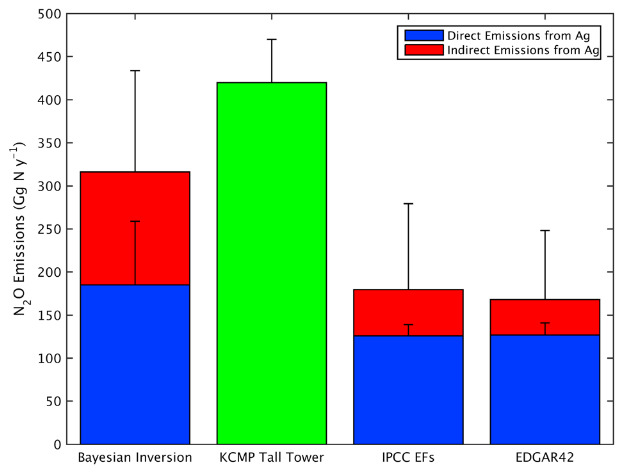

Figure 5. Comparison of N_2O budgets for the U.S. Corn Belt in year 2010 estimated using different methods (tall tower: boundary layer method at the KCMP tall tower [*Griffis et al.*, 2013]; IPCC EFs: estimate from IPCC EF method). Error bars indicate the uncertainties of regional budget estimate from direct and indirect emissions, respectively (the Bayesian inversion shows the N_2O budget from April to October in 2010, a total of 7 months; the KCMP tall tower, IPCC EFs, and EDGAR42 all show an annual budget).

excellent agreement with our Bayesian inverse analysis and slightly higher than that suggested by *Griffis et al*. [2013] and *Fassbinder et al*. [2013]. Using an independent approach, our analyses indicate that the both direct and indirect emissions are underestimated in the IPCC inventories and provide further support that the large disparity between top-down and bottom-up methodologies is likely due to poor constraints on indirect emissions.

It is estimated that on the order of 25–50% of the U.S. Corn Belt has been drained to support agricultural production [*U.S. Department of Agriculture*, 1987]. Although there is growing evidence that fine-scale drainage features are hot spots of indirect N_2O emissions [*Outram and Hiscock*, 2012; *Turner et al*., 2015], quantifying the spatiotemporal variation in these emission remains a challenge. The episodic nature and high spatial variability of these hot spots make them difficult to characterize and give rise to large uncertainties when integrating over space and time to obtain annual emission estimates. The Bayesian inverse model approach used here suggests a regional EF ranging from 0.018 to 0.038 for indirect emissions. In order to directly compare to IPCC EF related to leaching and runoff, we subtracted N_2O emissions from volatilization and redeposition. *Griffis et al*. [2013] used wet and dry N deposition (WDD) and the redeposition of local N (RDP) to represent indirect volatilization pathways. Multiplying WDD and RDP (a total of 3.1 Tg N yr^{-1}) by the IPCC indirect EF associated with volatilization (0.01, ranging from 0.002 to 0.05) gives an estimate of the N_2O budget from volatilization and redeposition of approximately 31 Gg N yr^{-1}. The indirect volatilization budget was then subtracted from the indirect emissions estimated from the Bayesian inversion to obtain the indirect emissions from leaching and runoff. The results indicate a regional EF ranging from 0.014 to 0.035 for indirect emissions related to leaching and runoff that is in relatively good agreement with that proposed by *Turner et al*. [2015]. They employed a chamber-based approach to measure riverine N_2O fluxes across stream orders ranging from fine-scale tile drainage to the Mississippi River. Interestingly, their data and analyses suggest a regional EF ranging from 0.007 to 0.03, which is in relatively close agreement with our inverse modeling approach. These independent approaches provide strong evidence that indirect emissions from drainage networks and streams within the U.S. Corn Belt are important sources and that their EF should be revised accordingly.

3.4. Environmental Controls on Direct and Indirect N_2O Emissions

Nitrogen availability and environmental factors including air temperature, soil moisture, precipitation, and surface runoff are important drivers of N_2O emissions [*Singurindy et al*., 2009; *Zona et al*., 2011; *Luo et al*., 2013]. Hourly weighted means of environmental variables of interest from WRF3.5 were computed for the entire study domain, with the weighting based on the intensity of the source footprint function for each grid cell and smoothed using a 24 h running mean. For the study period (May to September, 2010 and 2011), the mean air temperature was 15.6 and 16.2°C, respectively. The cumulative precipitation was 496 and 545 mm,

Table 3. Linear Regression Analyses of Environmental Factors and the Direct/Indirect Scaling Factors

	Scaling Factors			
	Direct Emissions		Indirect Emissions	
	r^2	p Value	r^2	p Value
Air temperature (T)	0.25	0.024	0.2	0.08
Soil Moisture (θ)	0.007	0.76	0.32	0.02
Surface runoff (R)	0.0001	0.97	0.33	0.01
Combined effect (T, θ, R)	0.26	0.02	0.44	0.0047

the mean soil water content was 0.32 and 0.39 kg/kg, and the cumulative surface runoff was 25.3 and 49.9 mm in 2010 and 2011, respectively. The larger cumulative precipitation in 2011 contributed to the high soil water content and surface runoff, with a soil water content and surface runoff that was 22% and 97% higher in 2011, respectively. Interestingly, both years showed similar direct emissions, while in 2011 the indirect emissions were 108% greater than in 2010.

To investigate how the interannual variations were driven with respect to important environmental factors, we applied biweekly Bayesian inverse analyses, from May to September in both 2010 and 2011. The Bayesian inversions permit retrieval of the scaling factors, indicating the amplitude of direct and indirect N_2O emissions, respectively. Combined with the 2 week mean environmental parameters, a linear regression analysis was conducted to investigate the correlations with direct/indirect emissions and the environmental variables (Table 3). We derived a multilinear regression model (MLR) that incorporated air temperature (T), soil water content (θ), and surface runoff (R) as explanatory variables using MATLAB (Matlab, Version R2015a, Mathworks, Natick, Massachusetts, USA). The MLR ($f(T, \theta, R)$) has the form

$$\boldsymbol{\Gamma} \approx \mathbf{f}(\mathbf{T}, \boldsymbol{\theta}, \mathbf{R}) = \mathbf{b_0} + \mathbf{b_1 T} + \mathbf{b_2} \boldsymbol{\theta} + \mathbf{b_3 R} \quad (6)$$

where Γ is the direct/indirect scaling factor.

The statistical analyses indicate that biweekly variability in direct emissions had a positive linear correlation with air temperature ($p = 0.024$, and $r^2 = 0.25$), but was not correlated with soil water content ($p = 0.76$) or surface runoff ($p = 0.97$). Mean air temperatures within the study period in 2010 and 2011 were similar and support why direct emissions were similar in both years.

The biweekly variability in indirect emissions show a moderate correlation with air temperature ($p = 0.08$, and $r^2 = 0.20$), strong correlation with soil water content ($p = 0.02$, and $r^2 = 0.32$), and surface runoff ($p = 0.01$, and $r^2 = 0.33$). The combined effect explains a significant amount ($p = 0.005$, and $r^2 = 0.44$) of the variability in the indirect emissions.

Short-term heavy precipitation is also an important factor contributing to wetter and anaerobic soil conditions and heavier surface runoff and therefore larger direct and indirect emissions [*Fassbinder et al.*, 2013]. For day of year (DOY) 121–135 and DOY 136–152 2011, the two time periods shared similar air temperature (16.8°C and 17.3°C, respectively), but the intense precipitation event during DOY 136–152 increased the cumulative precipitation from 30 mm to 127.7 mm. This event increased the soil water content by 13%, as well as cumulative surface runoff significantly from 3.0 mm to 11.7 mm. During this time period, the Bayesian inverse analysis indicated that direct and indirect emissions increased by 40% and 83%, respectively.

These findings, and related results from *Turner et al*. [2015], demonstrate that the offsite transport of N from farm fields is a dual environmental threat. The role of nitrate in the generation of hypoxia in water bodies is well known; its role as a precursor to substantial indirect emissions of N_2O has so far been less appreciated. The seriousness of both problems underscores the importance of reducing the leakage of reactive nitrogen in agricultural systems.

4. Conclusions

Based on high-precision N_2O tall tower observations and a novel Bayesian inversion method that partitions N_2O emissions into its direct and indirect components, we have shown the following:

1. N_2O emissions from agricultural sources within the Corn Belt were 319 ± 184 (total), 188 ± 66 (direct), and 131 ± 118 Gg N yr^{-1} (indirect) in 2010 versus 471 ± 326, 198 ± 80, and 273 ± 246 Gg N yr^{-1} in 2011. The direct and indirect emissions in 2011 increased 5% and 108%, respectively, compared to 2010 due to increased precipitation.
2. Direct and indirect N_2O emissions were out of phase. Indirect emissions reached a maximum in June, while direct emissions reached a maximum in July. This phase shift is attributed to a combination of spring-time fertilization throughout much of the Corn Belt and relatively high runoff that peaks in June.
3. Inverse modeling analyses support that the indirect emission factor associated with runoff and leaching ranges from 0.014 to 0.035 for the U.S. Corn Belt. This represents an upward adjustment of 1.9- to 4.6-fold relative to the Intergovernmental Panel on Climate Change and is in excellent agreement with recent bottom-up field studies.

Acknowledgments
Financial support for this research has been provided by the United States Department of Agriculture, grant USDA-NIFA 2013-67019-21364; USDA-ARS, NOAA (grant NA13OAR4310086); and MnDRIVE. We express our sincere thanks to Tom Nelson and Minnesota Public Radio for the logistical support at the KCMP tall tower. All models and analyses were performed at the Minnesota Supercomputing Institute for Advanced Computational Research. Data are hosted at http://www.biometeorology.umn.edu/research/data-archives.

References

Alexander, R. B., R. A. Smith, and G. E. Schwarz (2000), Effect of stream channel size on the delivery of nitrogen to the Gulf of Mexico, *Nature*, *403*, 758–762, doi:10.1038/35001562.

Baker, J. M., T. J. Griffis, and T. E. Ochsner (2012), Coupling landscape water storage and supplemental irrigation to increase productivity and improve environmental stewardship in the U.S. Midwest, *Water Resour. Res.*, *48*, W05301, doi:10.1029/2011WR011780.

Beaulieu, J. J., et al. (2011), Nitrous oxide emission from denitrification in stream and river networks, *Proc. Natl. Acad. Sci. U.S.A.*, *108*(1), 214–219, doi:10.1073/pnas.1011464108.

Bousquet, P., et al. (2011), Source attribution of the changes in atmospheric methane for 2006–2008, *Atmos. Chem. Phys.*, *11*(8), 3689–3700, doi:10.5194/acp-11-3689-2011.

Bouwman, A. F., K. W. Vanderhoek, and J. G. J. Oliver (1995), Uncertainties in the global source distribution of nitrous-oxide, *J. Geophys. Res.*, *100*, 2785–2800, doi:10.1029/94JD02946.

Carouge, C., P. Peylin, P. J. Rayner, P. Bousquet, F. Chevallier, and P. Ciais (2010), What can we learn from European continuous atmospheric CO_2 measurements to quantify regional fluxes—Part 2: Sensitivity of flux accuracy to inverse setup, *Atmos. Chem. Phys.*, *8*(5), 3119–3129, doi:10.5194/acpd-8-18621-2008.

Crutzen, P. J., A. R. Mosier, K. A. Smith, and W. Winiwarter (2008), N_2O release from agro-biofuel production negates global warming reduction by replacing fossil fuels, *Atmos. Chem. Phys.*, *8*, 389–395, 2008.

De Klein, C., R. S. A. Novoa, S. Ogle, K. A. Smith, P. Rochette, T. C. Wirth, B. G. McConkey, A. Mosier, and K. Rypdal (2006), N_2O emissions from managed soils, and CO_2 emissions from lime and urea application, in *2006 IPCC Guidelines for National Greenhouse Gas Inventories, Vol 4: Agriculture, Forestry and Other Land Use*, edited by H. S. Eggleston et al., pp. 11.11–11.54, Institute for Global Environmental Strategies (IGES), Intergovernmental Panel on Climate Change (IPPC), Kanagawa, Japan.

Del Grosso, S. J., T. Wirth, S. M. Ogle, and W. J. Parton (2008), Estimating agricultural nitrous oxide emissions, *Eos (Washington. DC).*, *89*(51), 529, doi:10.1029/2008EO510001.

DelGrosso, S. J., W. J. Parton, A. R. Mosier, D. S. Ojima, A. E. Kulmala, and S. Phongpan (2000), General model for N_2O and N_2 gas emissions from soils when comparing observed and gas emission rates from irrigated field soils used for model testing NO_2, *Global Biogeochem. Cycles*, *14*, 1045–1060, doi:10.1029/1999GB001225.

Dlugokencky, E. J., L. P. Steele, P. M. Lang, and K. A. Masarie (1994), The growth rate and distribution of atmospheric methane, *J. Geophys. Res.*, *99*(D8), 17021, doi:10.1029/94JD01245.

Fassbinder, J. J., N. M. Schultz, J. M. Baker, and T. J. Griffis (2013), Automated, low-power chamber system for measuring nitrous oxide emissions, *J. Environ. Qual.*, *42*, 606–14, doi:10.2134/jeq2012.0283.

Gerbig, C., J. C. Lin, S. C. Wofsy, B. C. Daube, A. E. Andrews, B. B. Stephens, P. S. Bakwin, and C. A. Grainger (2003), Toward constraining regional-scale fluxes of CO_2 with atmospheric observations over a continent: 1. Observed spatial variability from airborne platforms, *J. Geophys. Res.*, *108*(D24), 4756, doi:10.1029/2002JD003018.

Gómez, D. R., J. D. Watterson, B. B. Americano, C. Ha, G. Marland, E. Matsika, L. N. Namayanga, B. Osman-Elasha, J. D. Kalenga Saka, and K. Treanton (2006), IPCC guidelines for national greenhouse gas inventories, *Institute for Global Environmental Strategies, Kamiyamaguchi Hayama, Japan*.

Grace, P. R., G. Philip Robertson, N. Millar, M. Colunga-Garcia, B. Basso, S. H. Gage, and J. Hoben (2011), The contribution of maize cropping in the Midwest USA to global warming: A regional estimate, *Agric. Syst.*, *104*(3), 292–296, doi:10.1016/j.agsy.2010.09.001.

Griffis, T. J., J. M. Baker, S. D. Sargent, M. Erickson, J. Corcoran, M. Chen, and K. Billmark (2010), Influence of C_4 vegetation on $^{13}CO_2$ discrimination and isoforcing in the upper Midwest, United States, *Global Biogeochem. Cycles*, *24*, GB4006, doi:10.1029/2009GB003768.

Griffis, T. J., X. Lee, J. M. Baker, M. P. Russelle, X. Zhang, R. Venterea, and D. B. Millet (2013), Reconciling the differences between top-down and bottom-up estimates of nitrous oxide emissions for the U.S. Corn Belt, *Global Biogeochem. Cycles*, *27*, 746–754, doi:10.1002/gbc.20066.

Heald, C. L., D. J. Jacob, D. B. A. Jones, P. I. Palmer, J. A. Logan, D. G. Streets, G. W. Sachse, J. C. Gille, R. N. Hoffman, and T. Nehrkorn (2004), Comparative inverse analysis of satellite (MOPITT) and aircraft (TRACE-P) observations to estimate Asian sources of carbon monoxide, *J. Geophys. Res.*, *109*, D23306, doi:10.1029/2004JD005185.

Hinshaw, S. E., and R. A. Dahlgren (2013), Dissolved nitrous oxide concentrations and fluxes from the eutrophic San Joaquin River, California, *Environ. Sci. Technol.*, *47*(3), 1313–1322, doi:10.1021/es301373h.

Homer, C. G., J. A. Dewitz, L. Yang, S. Jin, P. Danielson, G. Xian, J. Coulston, N. D. Herold, J. D. Wickham, and K. Megown (2011), Completion of the 2006 National Land Cover Database for the conterminous United States, *Photogramm. Eng. Remote Sens.*, *77*(Figure 1), 858–566.

Hong, S.-Y., J. Dudhia, and S.-H. Chen (2004), A revised approach to ice microphysical processes for the bulk parameterization of clouds and precipitation, *Mon. Weather Rev.*, *132*(1), 103–120, doi:10.1175/1520-0493(2004)132<0103:ARATIM>2.0.CO;2.

Hong, S.-Y., Y. Noh, and J. Dudhia (2006), A new vertical diffusion package with an explicit treatment of entrainment processes, *Mon. Weather Rev.*, *134*(9), 2318–2341, doi:10.1175/MWR3199.1.

Hu, L., et al. (2015), Emissions of C_6-C_8 aromatic compounds in the United States: Constraints from tall tower and aircraft measurements, *J. Geophys. Res. Atmos.*, *120*, 826–842, doi:10.1002/2014JD022627.

Janjic, Z. (2002), Nonsingular Implementation of the Mellor-Yamada Level 2.5 Scheme in the NCEP Meso model, *Natl. Centers Environ. Predict.*, 61.

Jeong, S., C. Zhao, A. E. Andrews, L. Bianco, J. M. Wilczak, and M. L. Fischer (2012), Seasonal variation of CH_4 emissions from central California, *J. Geophys. Res.*, *117*, D11306, doi:10.1029/2011JD016896.

Kain, J. S. (2004), The Kain–Fritsch convective parameterization: An update, *J. Appl. Meteorol.*, *43*(1), 170–181, doi:10.1175/1520-0450(2004)043<0170:TKCPAU>2.0.CO;2.

Kim, S. Y., D. B. Millet, L. Hu, M. J. Mohr, T. J. Griffis, D. Wen, J. C. Lin, S. M. Miller, and M. Longo (2013), Constraints on carbon monoxide emissions based on tall tower measurements in the U.S. upper Midwest, *Environ. Sci. Technol.*, *47*(15), 8316–8324, doi:10.1021/es4009486.

Kort, E. A., J. Eluszkiewicz, B. B. Stephens, J. B. Miller, C. Gerbig, T. Nehrkorn, B. C. Daube, J. O. Kaplan, S. Houweling, and S. C. Wofsy (2008), Emissions of CH_4 and N_2O over the United States and Canada based on a receptor-oriented modeling framework and COBRA-NA atmospheric observations, *Geophys. Res. Lett.*, *35*, L18808, doi:10.1029/2008GL034031.

Kretschmer, R., F. T. Koch, D. G. Feist, G. Biavati, U. Karstens, and C. Gerbig (2012), Toward assimilation of observation-derived mixing heights to improve atmospheric tracer transport models, *Geophys. Monogr. Ser.*, *200*, 185–205, doi:10.1029/2012GM001255.

Lin, J. C., and C. Gerbig (2005), Accounting for the effect of transport errors on tracer inversions, *Geophys. Res. Lett.*, *32*, 1–5, doi:10.1029/2004GL021127.

Lin, J. C., C. Gerbig, S. C. Wofsy, A. E. Andrews, B. C. Daube, K. J. Davis, and C. A. Grainger (2003), A near-field tool for simulating the upstream influence of atmospheric observations: The Stochastic Time-Inverted Lagrangian Transport (STILT) model, *J. Geophys. Res.*, *108*(D16), 4493, doi:10.1029/2002JD003161.

Lin, J. C., C. Gerbig, S. C. Wofsy, A. E. Andrews, B. C. Daube, C. A. Grainger, B. B. Stephens, P. S. Bakwin, and D. Y. Hollinger (2004), Measuring fluxes of trace gases at regional scales by Lagrangian observations: Application to the CO_2 Budget and Rectification Airborne (COBRA) study, *J. Geophys. Res.*, *109*, D15304, doi:10.1029/2004JD004754.

Luo, G. J., R. Kiese, B. Wolf, and K. Butterbach-Bahl (2013), Effects of soil temperature and moisture on methane uptake and nitrous oxide emissions across three different ecosystem types, *Biogeosciences*, *10*(5), 3205–3219, doi:10.5194/bg-10-3205-2013.

Matross, D. M., et al. (2006), Estimating regional carbon exchange in New England and Quebec by combining atmospheric, ground-based and satellite data, *Tellus, Ser. B Chem. Phys. Meteorol.*, *58*(5), 344–358, doi:10.1111/j.1600-0889.2006.00206.x.

Mikaloff Fletcher, S. E., P. P. Tans, L. M. Bruhwiler, J. B. Miller, and M. Heimann (2004), CH_4 sources estimated from atmospheric observations of CH_4 and its $^{13}C/^{12}C$ isotopic ratios: 2. Inverse modeling of CH_4 fluxes from geographical regions, *Global Biogeochem. Cycles*, *18*, GB4005, doi:10.1029/2004GB002224.

Millar, N., G. Philip Robertson, P. R. Grace, R. J. Gehl, and J. P. Hoben (2010), Nitrogen fertilizer management for nitrous oxide (N_2O) mitigation in intensive corn (Maize) production: An emissions reduction protocol for US Midwest agriculture, *Insectes Soc.*, *57*(2), 185–204, doi:10.1007/s11027-010-9212-7.

Miller, S. M., et al. (2008), Sources of carbon monoxide and formaldehyde in North America determined from high-resolution atmospheric data, *Atmos. Chem. Phys. Discuss.*, *8*(3), 11,395–11,451, doi:10.5194/acpd-8-11395-2008.

Miller, S. M., et al. (2012), Regional sources of nitrous oxide over the United States: Seasonal variation and spatial distribution, *J. Geophys. Res.*, *117*(6), 1–13, doi:10.1029/2011JD016951.

Myhre, G., et al. (2013), Anthropogenic and natural radiative forcing. In *Climate Change 2013: The Physical Science Basis. Contribution of Working Group I to the Fifth Assessment Report of the Intergovernmental Panel on Climate Change*, edited by T. F. Stocker et al., pp. 659–740, Cambridge Univ. Press., Cambridge and New York, doi:10.1017/CBO9781107415324.018.

Nehrkorn, T., J. Eluszkiewicz, S. C. Wofsy, J. C. Lin, C. Gerbig, M. Longo, and S. Freitas (2010), Coupled weather research and forecasting-stochastic time-inverted lagrangian transport (WRF-STILT) model, *Meteorol. Atmos. Phys.*, *107*(1), 51–64, doi:10.1007/s00703-010-0068-x.

Nevison, C. (2000), Review of the IPCC methodology for estimating nitrous oxide emissions associated with agricultural leaching and runoff, *Chemosph. - Glob. Chang. Sci.*, *2*(3-4), 493–500, doi:10.1016/S1465-9972(00)00013-1.

Oleson, K. W., D. M. Lawrence, B. Gordon, M. G. Flanner, E. Kluzek, J. Peter, S. Levis, S. C. Swenson, E. Thornton, and J. Feddema (2013), Technical description of version 4.5 of the Community Land Model (CLM), *NCAR/TN-503+STR NCAR Tech. Note*, (July), 266, doi:10.5065/D6RR1W7M.

Outram, F. N., and K. M. Hiscock (2012), Indirect nitrous oxide emissions from surface water bodies in a lowland arable catchment: A significant contribution to agricultural greenhouse gas budgets?, *Environ. Sci. Technol.*, *46*(15), 8156–8163, doi:10.1021/es3012244.

Parton, W. J., A. R. Mosier, D. S. Ojima, D. W. Valentine, D. S. Schimel, K. Weier, and A. E. Kulmala (1996), Generalized model for N_2 and N_2O production from nitrification, Global Biogeochem. *Cycles*, *10*(3), 401–412.

Parton, W., E. Holland, S. Del Grosso, D. Hartman, M. Martin, A. Mosier, D. Ojima, and D. Schimel (2001), Generalized model for NO_x and N_2O emissions from soils, *J. Geophys. Res.*, *106*, 17,403–17,419, doi:10.1029/2001JD900101.

Rodgers, C. D. (2000), *Inverse Methods for Atmospheric Sounding: Theory and Practice*, vol. 2, pp. 256 , World scientific, Singapore.

Saikawa, E., C. A. Schlosser, and R. G. Prinn (2013), Global modeling of soil nitrous oxide emissions from natural processes, *Global Biogeochem. Cycles*, *27*, 972–989, doi:10.1002/gbc.20087.

Shcherbak, I., N. Millar, and G. P. Robertson (2014), Global metaanalysis of the nonlinear response of soil nitrous oxide (N_2O) emissions to fertilizer nitrogen, *Proc. Natl. Acad. Sci. U.S.A.*, *111*(25), 9199–204, doi:10.1073/pnas.1322434111.

Singurindy, O., M. Molodovskaya, B. K. Richards, and T. S. Steenhuis (2009), Nitrous oxide emission at low temperatures from manure-amended soils under corn (Zea mays L.), *Agric. Ecosyst. Environ.*, *132*(1-2), 74–81, doi:10.1016/j.agee.2009.03.001.

Smith, K. A., A. R. Mosier, P. J. Crutzen, and W. Winiwarter (2012), The role of N_2O derived from crop-based biofuels, and from agriculture in general, in Earth's climate, *Philos. Trans. R. Soc. Lon.. B. Biol. Sci.*, *367*(1593), 1169–74, doi:10.1098/rstb.2011.0313.

Thompson, R. L., et al. (2014), Nitrous oxide emissions 1999 to 2009 from a global atmospheric inversion, *Atmos. Chem. Phys.*, *14*(4), 1801–1817, doi:10.5194/acp-14-1801-2014.

Turner, P. A., T. J. Griffis, X. Lee, J. M. Baker, R. T. Venterea, and J. D. Wood (2015), Indirect nitrous oxide emissions from streams within the US Corn Belt scale with stream order, *Proc. Natl. Acad. Sci.*, *112*(32), 9839–9843, doi:10.1073/pnas.1503598112.

U.S. Department of Agriculture (1987), Farm drainage in the United States, *Tech. Rep.*, United States Department of Agriculture Miscellaneous Publication 1455.

Wells, K. C., et al. (2015), Simulation of atmospheric N_2O with GEOS-Chem and its adjoint: Evaluation of observational constraints, *Geosci. Model Dev.*, *8*(10), 3179–3198, doi:10.5194/gmd-8-3179-2015.

Werle, P., R. Mücke, and F. Slemr (1993), The limits of signal averaging in atmospheric trace-gas monitoring by tunable diode-laser absorption spectroscopy (TDLAS), *Appl. Phys. B Photophysics Laser Chem.*, *57*(2), 131–139, doi:10.1007/BF00425997.

Zhang, X., X. Lee, T. J. Griffis, J. M. Baker, and W. Xiao (2014), Estimating regional greenhouse gas fluxes: An uncertainty analysis of planetary boundary layer techniques and bottom-up inventories, *Atmos. Chem. Phys.*, *14*(19), 10,705–10,719, doi:10.5194/acp-14-10705-2014.

Zhao, C., A. E. Andrews, L. Bianco, J. Eluszkiewicz, A. Hirsch, C. MacDonald, T. Nehrkorn, and M. L. Fischer (2009), Atmospheric inverse estimates of methane emissions from central California, *J. Geophys. Res.*, *114*, D16302, doi:10.1029/2008JD011671.

Zona, D., I. A. Janssens, M. S. Verlinden, L. S. Broeckx, J. Cools, B. Gioli, A. Zaldei, and R. Ceulemans (2011), Impact of extreme precipitation and water table change on N_2O fluxes in a bio-energy poplar plantation, *Biogeosciences Discuss.*, *8*(2), 2057–2092, doi:10.5194/bgd-8-2057-2011.